Cytoplasmic trafficking of IGF-II mRNA-binding protein by conserved KH domains

Finn C. Nielsen[1], Jacob Nielsen[2], Mette A. Kristensen[2], Grete Koch[1] and Jan Christiansen[2,*]

[1]Department of Clinical Biochemistry, Rigshospitalet, Copenhagen, Denmark
[2]Institute of Molecular Biology, University of Copenhagen, Denmark
*Author for correspondence (e-mail: janchr@mermaid.molbio.ku.dk)

Accepted 25 February 2002
Journal of Cell Science 115, 2087-2097 (2002) © The Company of Biologists Ltd

Summary

The IGF-II mRNA-binding proteins (IMPs), which are composed of two RNA recognition motifs, (RRM) and four hnRNP K homology (KH) domains, have been implicated in subcytoplasmic localization of mRNAs during embryogenesis. The IMP family originated via two gene duplications before the divergence of vertebrates, and IMP homologues consisting of only the four KH motifs have been identified in *Drosophila* and *Caenorhabditis elegans.* Here we characterise the trafficking of GFP-IMP1 fusion proteins and determine the structural determinants for proper cytoplasmic localization. GFP-IMP1 is present in large 200-700 nm RNP granules, which are distributed along microtubules. In motile cells, GFP-IMP1 is transported towards the leading edge into the cortical region of the lamellipodia where it is connected to microfilaments. Granules travel in an ATP-dependent fashion at an average speed of 0.12 μm/s (range 0.04-0.22 μm/s), and cells switch from a delocalized to a localized pattern within 15-20 minutes. Both granule formation and localization are unaffected by removal of the two RRMs, whereas deletion of the KH domains, which mediate RNA-binding, impairs these functions. We conclude that IMP1 localization is associated with motility and that the major functions of IMP1 are carried out by the phylogenetically conserved KH domains.

Key words: Cytoskeleton, Microtubules, RNA localization, RNP granules, Zipcode-binding protein

Introduction

RNA localization is a conserved mechanism for polarizing genetic information in the establishment of asymmetries during embryogenesis and adult life. The salient feature behind this mechanism is the ability to transport mRNAs in a repressed form, thus enabling local protein synthesis at final destinations within the cell. RNA localization may involve RNA-binding proteins, motor proteins and cytoskeletal organizers. Yeast *ASH1* mRNA is localized in an actin- and myosin-dependent manner during cell budding by the participation of a motor protein (Myo4p), an RNA-binding protein (She2p), an adaptor (She3p) and two organizers of the actin cytoskeleton (reviewed by Kwon and Schnapp, 2001). In metazoans, the *Drosophila* oocyte provides additional striking examples of RNA localization, since the two main body axes of the embryo are determined by the positions of three specific mRNAs – *bicoid*, *oskar* and *nanos* (reviewed in van Eeden and St Johnston, 1999). The microtubule-dependent localization of both *bicoid* and *oskar* mRNAs to the anterior and posterior poles, respectively, requires the activity of the double-stranded RNA-binding protein Staufen (St Johnston et al., 1991). In mammals, there are also examples of asymmetric localization of mRNAs in terminally differentiated cells in the brain, but here the molecular components of RNA trafficking are only beginning to emerge. The microtubule-dependent localization of myelin basic protein mRNA to the oligodendrocyte processes seems to depend on hnRNP A2, which binds to a cis-element in the 3′ UTR (Hoek et al., 1998). Moreover, the human Staufen homologue has been shown to be present in RNA-containing granules in transit to neuronal dendrites in a microtubule-dependent manner, but the RNA-targets are not known (Kohrmann et al., 1999).

During a search for trans-acting factors associating with IGF-II mRNAs, we recently identified a family of three IGF-II mRNA-binding proteins (IMP1, IMP2 and IMP3), which exhibit multiple attachments to IGF-II leader 3 mRNA and the reciprocally imprinted H19 RNA (Nielsen et al., 1999; Runge et al., 2000). IMP3 is orthologous to the *Xenopus* Vg1 RNA-binding protein (Vg1RBP/Vera), which mediates the localization of Vg1 mRNA to the vegetal pole of the oocyte during oocyte maturation, and IMP1 is orthologous to the chicken zipcode-binding protein (ZBP-1), which participates in the localization β-actin mRNA to the leading edge of motile cells (Deshler et al., 1998; Havin et al., 1998; Ross et al., 1997). Moreover, IMP1 is orthologous to the mouse c-myc coding region determinant-binding protein, which may play a role in stabilisation of c-myc mRNA (Doyle et al., 1998). IMPs contain the unique combination of two RNA recognition motifs (RRMs) and four hnRNP K homology (KH) domains. The vertebrate IMP family originated by two gene duplications, shortly before the divergence of vertebrates (Spring, 1997), and IMP homologues consisting of only the four KH motifs have been identified in *Drosophila* (Nielsen et al., 2000) and *Caenorhabditis elegans* (accession number T23837). Mouse IMPs are produced in a burst at embryonic day 12.5 followed by a decline towards birth, and they are co-expressed with IGF-II mRNA and H19 RNA in developing epithelia, muscle and placenta in both mouse and human embryos (Nielsen et al.,

1999). IMP is mainly cytoplasmic and the immunocytochemical appearance ranges from a distinct concentration in perinuclear regions and lamellipodia to a completely delocalized pattern (Nielsen et al., 1999). H19 RNA colocalizes with IMP, and removal of the high-affinity attachment site led to delocalization of the truncated RNA (Runge et al., 2000), indicating that IMPs are involved in cytoplasmic trafficking of RNA.

In the present study, we have characterised the dynamic subcytoplasmic localization of GFP-IMP1 fusion proteins and determined the structural features that are sufficient for proper transport and cytoplasmic granule formation.

Materials and Methods

Plasmid constructs

pEGFP-IMP1 and pECFP-IMP1 were generated by inserting the open reading frame of human IMP1 into the *Bgl*II and *Eco*RI site of the pEGFP-C1 and pECFP-C1 vectors (Clontech, USA). For construction of the pBABEGFP-IMP1 retroviral vector, an *Nhe*I-*Xba*I fragment of GFP-IMP1 was taken from pEGFP-IMP1 and cloned into the *Xba*I site of pGEM11 before it was inserted at the *Bam*HI and *Eco*RI sites of pBABE puro (Morgenstern and Land, 1990). IMP1 deletion mutants were generated by PCR and cloned into the *Eco*RI and *Bam*HI sites of pEGFP-C2, pEYFP-C2 or pECFP-C2. pYFP-KDEL and pYFP-β1,4-galactosyltransferase constructs for visualization of the endoplasmic reticulum and Golgi compartments, respectively, were obtained from Clontech, USA. Acid vesicles were monitored by Lysotracker TxRed DND99 from Molecular Probes, USA.

Cell culture, transfections and imaging

Mouse NIH 3T3 embryo fibroblast cells were obtained from the American Type Culture Collection and routinely maintained in RPMI 1640 medium supplemented with 10% fetal calf serum or in Dulbecco's modified Eagle's medium containing 10% calf serum. Cells were transiently transfected with LipofectAMINE 2000 (Life Technologies Inc., USA) according to the manufacturer's instructions. Briefly, 30,000 cells/cm^2 were seeded on glass plates or laminin-coated plates 24 hours prior to transfection. Cells were transfected with 2 μg/ml of the indicated plasmid and left for 48 hours before they were examined. NIH 3T3 cells stably expressing GFP-IMP1 were generated by retrovirus-mediated insertion of the pBABE-GFP-IMP1, as described previously (Morgenstern and Land, 1990). The distribution of GFP-IMP and cellular markers in living and fixed cells (see below) was examined with a Zeiss LSM 510 confocal laser scanning microscope. During time-lapse photography and photobleaching experiments, cells were kept in HEPES-buffered RPMI 1640 medium supplemented with 10% fetal calf serum at 36°C. Fluorescence recovery after photobleaching (FRAP) was determined by assessment of the total fluroescence recovery in the bleached area at 20 second intervals. In ATP depletion experiments, the cells were incubated with 0.05% sodium azide and 25 mM 2-deoxyglucose for 30 minutes prior to FRAP.

Immunocytochemistry

Cells were fixed for 10 minutes at room temperature with 3.7% formaldehyde and washed three times with phosphate-buffered saline (PBS) with 0.1% Triton X-100. After treatment with 0.1% BSA in PBS for 30 minutes, cells were incubated with anti-vimentin antibody at 1:100 (Santa Cruz Biotechnology, USA) or anti-tubulin antibody at 1:200 (Sigma-Aldrich, USA). After washing with PBS, cells were finally incubated with donkey rhodamine red-x-conjugated secondary anti-goat or mouse antibody (Jackson Laboratories, USA) for 30 minutes and washed. F-actin staining was performed with Texas-Red-conjugated phalloidin for 1 hour in 0.1% BSA in PBS according to the manufacturer's instruction (Molecular Probes, USA).

UV crosslinking

A frozen cell pellet of approximately 5×10^7 NIH 3T3 cells or NIH 3T3 cells stably expressing GFP-IMP1 was resuspended in 1 ml of lysis buffer (20 mM Tris-HCl, pH 8.0, 140 mM KCl, 1.5 mM $MgCl_2$, 0.5% Nonidet P-40 (NP-40), 0.5 mM dithiothreitol (DTT) and centrifuged at 14,000 ***g*** for 10 minutes at 4°C. Glycerol was added to the supernatant at a final concentration of 5%, and the cytoplasmic extract was stored at –80°C in aliquots containing 5-7 μg of protein per μl. Radiolabelled IGF-II leader 3 segment C mRNA (Nielsen et al., 1999) was synthesised to a specific activity of 30 Ci of uridine/mmol. NIH 3T3 extract containing 15 μg of protein was incubated with 100 nCi of leader 3 segment C RNA for 25 minutes at room temperature in 10 μl of 20 mM Tris-HCl (pH 8.0), 140 mM KCl, 4 mM $MgCl_2$, 0.75 mM DTT, 0.1% NP-40, 0.1 μg/μl *Escherichia coli* tRNA. Samples were irradiated with 254 nm wavelength light for 30 minutes at 5.4 J/cm^2 on ice in a Stratalinker 1800 (Stratagene, USA). Excess probe was removed by digestion with 0.5 μg of RNase A at 37°C for 25 minutes. Samples were analysed by 10% polyacrylamide-sodium dodecyl sulfate (SDS) gel electrophoresis followed by autoradiography.

Mobility-shift analysis

In a final volume of 10 μl, 0.5 pmol of radiolabelled RNA (2 nCi) were incubated with recombinant IMP-1, RRM1-2, KH1-4, KH1-2 or KH 3-4 for 20 minutes at 30°C in 20 mM Tris-HCl (pH 8.0), 150 mM KCl, 2 mM $MgCl_2$, 5% glycerol, 0.1% Triton X-100, 0.004% bromophenolblue, 2 units RNasin and 0.01 μg/μl *E. coli* tRNA. Samples were chilled on ice and 1 μl of 10% Ficoll-400 was added. The non-denaturing gel electrophoresis was carried out in a 5% polyacrylamide gel containing 90 mM Tris-borate (pH 8.3), 50 mM KCl and 2 mM $MgCl_2$ at 4°C and 80 V for 6 hours. The recombinant proteins were expressed and purified as described (Nielsen et al., 1999), except that washing of chitin-beads was carried out in the presence of 1 M NaCl before cleavage with dithiothreitol.

Gradient centrifugations and blots

NIH 3T3 cells that stably express GFP-IMP1 (3×10^7 cells) were lysed in 500 μl 20 mM Tris-HCl (pH 8.5), 1.5 mM $MgCl_2$, 140 mM KCl, 0.5 mM DTT, 0.5% NP-40, 1000 U of RNasin (Promega) per ml and 0.1 mM cycloheximide. The lysate was centrifuged at 10,000 ***g*** for 10 minutes, and the supernatant was applied to a linear 20 to 47% sucrose gradient in 20 mM Tris-HCl (pH 8.0), 140 mM KCl, 5 mM $MgCl_2$. Centrifugation was carried out at 200,000 ***g*** for 2 hours 15 minutes in a Beckman SW 41 rotor.

5×10^7 frozen RD rhabdomyosarcoma cells were homogenized, and the undiluted lysate was centrifuged at 10,000 ***g*** for 5 minutes. The supernatant was applied to a linear 10-60% Nycodenz gradient in 20 mM HEPES-KOH (pH 7.3), 115 mM KCl. Centrifugation was carried out at 150,000 ***g*** for 16 hours at 4°C in a Beckman SW 41 rotor.

Fractions of 1 ml were collected, followed either by precipitation of sedimenting proteins in 10% trichloroacetic acid and western analysis or by precipitation of RNA and slot-blot analysis. Proteins were separated in a 10% polyacrylamide-SDS gel and transferred to polyvinyl difluoride Immobilon-P membranes (Millipore-Amicon, USA). After blocking, filters were incubated overnight at 4°C with anti-calnexin antibody (Santa Cruz Biotechnology, USA) or anti-IMP1 (Nielsen et al., 1999) in blocking solution and with horseradish-peroxidase-conjugated anti-rabbit immunoglobulin G (IgG) in

blocking solution for 1 hour at room temperature. Bound antibody was detected with enhanced chemiluminescence reagents according to the manufacturer's instructions (Pierce, USA). Total RNA in each fraction was hybridised with an IGF-II leader 3-specific probe as described previously (Nielsen et al., 1995).

Recombinant ^{32}P-labelled IMP1

For labelling of recombinant IMP1, an HMK-site was inserted close to the C-terminus. The open reading frame of human IMP1 was amplified by PCR using the upstream primer 5′-GGAATACCATATGAACAAGCTTTACATC-3′ and the downstream 5′-GGACCAGCTCTTCCGCACTTCCTCCGTGCCACGGACGCG-CGACGCTGTCCCTTCTGATGCT-3′ primer, which contains the HMK-site. The product was inserted into the *Nde*I and *Sap*I sites of pTYB1 and IMP1-HMK was expressed in *E. coli* and purified as described previously (Nielsen et al., 1999). Mobility-shift analysis confirmed that IMP1-HMK binds to RNA with the same affinity as wild-type IMP1. HMK-catalysed ^{32}P-labelling of IMP1-HMK was performed while IMP1-HMK was attached to the chitin-beads (Jensen et al., 1995). The beads were washed five times with 20 mM HEPES-KOH, pH 7.9, 200 mM NaCl and 20% glycerol and the labelled protein was isolated as described (Nielsen et al., 1999).

Pull-down of ^{32}P-labelled IMP1 with polymerised tubulin and actin

Binding of HMK-IMP1 to microtubules was examined with a Microtubule Associated Protein Spin-Down, Assay Kit (Cytoskeleton Inc., USA), according to the manufacturer's instructions, except that 0.2% Triton X-100 was included throughout the assay to prevent aggregation. Briefly, 1 nCi of ^{32}P-labelled IMP1-HMK was prespun at 164,000 ***g*** in a Beckman Airfuge for 15 minutes at room temperature in the presence of 6 μg BSA. The supernatant was added to 10 nM polymerised pure tubulin (20 μM dimers) in the absence or presence of MAPs (Cytoskeleton Inc. catalogue reference: MAPF or MAP2) for 20 minutes at room temperature in a total volume of 50 μl. Samples were centrifuged through a 100 μl 20% (w/v) sucrose cushion at 164,000 ***g*** for 25 minutes at room temperature. Pellets were resuspended in SDS load buffer and analysed by 10% SDS-PAGE followed by staining with Coomassie brilliant blue and autoradiography.

IMP1-HMK association with polymerised actin was analysed using an actin polymerisation kit (Cytoskeleton Inc., USA). Briefly, 6 nCi of ^{32}P-labelled IMP1-HMK in 50 μl 5 mM Tris-HCl, pH 8.0, 0.2 mM $CaCl_2$, 0.002% chlorhexidine was centrifuged for 150,000 ***g*** for 1 hour at room temperature in a Beckman Airfuge. 10 μl of supernatant was mixed with either 40 μl actin polymerisation buffer (5 mM Tris-HCl, pH 8.0, 50 mM KCl, 2 mM $MgCl_2$, 1 mM ATP, 0.2 mM $CaCl_2$, 0.002% chlorhexidine) or 40 μl of 1 μg/μl polymerised actin in actin polymerisation buffer. A positive control with actin and actinin at 0.2 μg/μl was included. Samples were incubated for 30 minutes at room temperature, followed by centrifugation for 1.5 hours at 150,000 ***g***. Pellets were resuspended in SDS load buffer, whereas 15 μl of 4× SDS load buffer was added to the supernatant. Samples were analysed in 10% SDS-PAGE gels followed by staining with Coomassie brilliant blue and autoradiography.

Surface plasmon resonance

Binding of microtubule-associated proteins to recombinant *Drosophila* IMP and human IMP1 domains was examined with a Biacore surface plasmon resonance apparatus (Biacore, Sweden). The *Drosophila* IMP (dIMP) or segments corresponding to RRM1-2 and KH1-4 were inserted in the *Bam*HI and *Eco*RI sites of pET28 (Novagen) and expressed in *E. coli* BL21/DE3 cells containing pRI952 (Nielsen et al., 1999). The His-tagged RRM1-2, KH1-4 and *Drosophila* IMP (dIMP) were purified under native conditions according to the manufacturer's instructions, and about 6000 resonance units were immobilized on a CM5 sensorchip by carbodiimide coupling. Phosphocellulose-purified tubulin, MAP-enriched tubulin and MAPs isolated by phosphocellulose chromatography were obtained from Cytoskeleton Inc., USA. 1 μl of each of the protein preparations were diluted in 100 μl 10 mM HEPES-KOH, pH 7.4, 150 mM NaCl, 3 mM EDTA and 0.005% (v/v) polysorbate 20. Samples were injected at a flow of 20 μl/minute over 5 minutes. The surface was reconstituted by washing in 0.2 M glycine for 30 seconds.

Results

A GFP-IMP1 fusion protein and endogenous IMP1 exhibit similar RNA-binding and sedimentation behaviours

Subcytoplasmic trafficking and anchoring of IMP1 were examined by expression of the N-terminal fusion protein GFP-IMP1 either in stably or transiently transfected NIH 3T3 fibroblasts. To evaluate the ability of the fusion protein to represent the function of the endogenous protein, we performed a UV crosslinking experiment with crude lysate from cells that stably express GFP-IMP1, and we determined the sedimentation of GFP-IMP1 compared with endogenous IMP1. Full-length IGF-II leader 3 segment C RNA, which is a high-affinity IMP1 RNA-target (Nielsen et al., 1999), was randomly ^{32}P-labelled and subjected to UV light at 254 nm in the presence of a cytoplasmic extract from NIH 3T3 cells. Fig. 1A shows the autoradiograph from the resulting SDS-polyacrylamide gel electrophoresis. IGF-II leader 3 segment C RNA was crosslinked to four major proteins with apparent molecular masses of 100 kDa, 69 kDa, 60 kDa and 50 kDa, as previously described (Nielsen et al., 1999). In the stable transfectants, an additional band of 95 kDa corresponding to the GFP-IMP1 fusion protein was visible. The ratio between GFP-IMP1 and endogenous IMP1 bands in the crosslinking assay correspond to the ratio observed in the western blot (Fig. 1B), indicating that GFP-IMP1 and endogenous IMP1 bind to RNA with a similar affinity. Moreover, the GFP-IMP1 band exhibits the same competition profile towards homopolymers as IMP1 (results not shown).

We previously found that IMP1 in human rhabdomyosarcoma cells was located in particles that sedimented at a rate of 40-150S (Nielsen et al., 1999). Western analysis with anti-IMP1 antibody of fractions from a 20-47% sucrose gradient showed that GFP-IMP1 co-sedimented with endogenous IMP1 (Fig. 1B). From the western analysis of the Mg^{2+}-containing gradient, it is estimated that the amount of GFP-IMP1 is about twice that of endogenous IMP1, which is expressed at a relatively low level in NIH 3T3 cells. We infer that GFP-IMP1 exhibits a similar mRNP distribution to endogenous IMP1.

Cytoplasmic trafficking of GFP-IMP1

The cytoplasmic localization and appearance of GFP-IMP1 in NIH 3T3 cells stably expressing this protein were examined by confocal microscopy of living cells. In resting cells, GFP-IMP1 was present in large granules, which were diffusely distributed in about 90% of the cells (Fig. 2A, frame 1). In the remaining cells, GFP-IMP1 accumulated in lamellipodia, near the leading

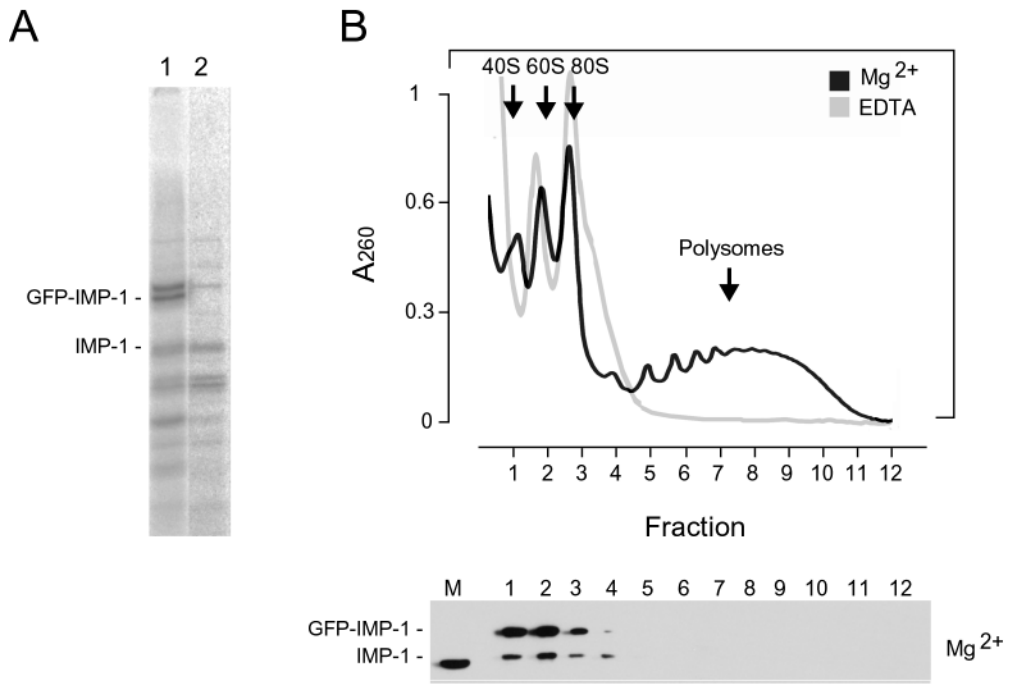

Fig. 1. RNA binding and subcellular distribution of GFP-IMP1. (A) UV crosslinking of IGF-II leader 3 segment C RNA with extract from either NIH 3T3 cells that stably express GFP-IMP1 (lane 1) or from normal NIH 3T3 cells (lane 2). (B) Cytoplasmic lysate from GFP-IMP1-expressing NIH 3T3 cells was separated in a 20-47% sucrose gradient. The upper panel shows the A_{260} sedimentation profile of ribosomal subunits and polyribosomes, and the lower panel shows the western analysis of the 12 fractions from the Mg^{2+}-containing gradient with anti-IMP1 antibody to IMP1 and GFP-IMP1. M is a lane with recombinant IMP1.

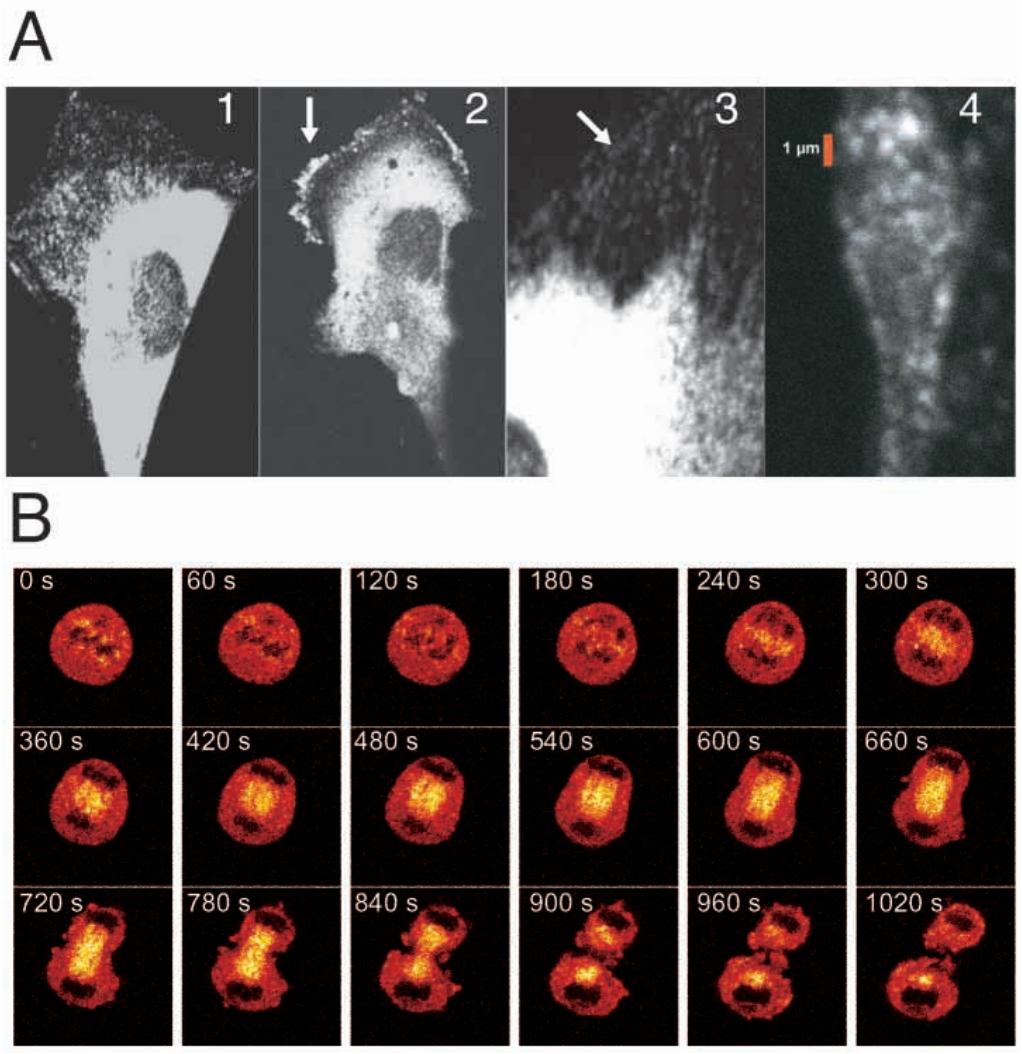

Fig. 2. Cytoplasmic localization of GFP-IMP1 during interphase and anaphase in NIH 3T3 cells. (A) Cytoplasmic localization of GFP-IMP1 during interphase. (1) A cell with a delocalised granular pattern of fluorescence that is typically seen in cells seeded on glass plates. (2) A migrating cell with GFP-IMP1 localized to the leading edge (arrow). (3,4) The GFP-IMP1-containing granules. (B) Time-lapse microscopy of GFP-IMP1 during mitosis displayed in glow scale.

edge and around the nucleus (Fig. 2A, frame 2). After seeding on laminin-coated plates, which stimulate spreading and migration of the cells, GFP-IMP1 was localized in about 40% of the cells. Both cells with localized and cells with evenly distributed GFP-IMP1 exhibit granules that are often arranged in rows along the cytoskeleton (Fig. 2A, frame 3). The apparent optical diameter of the granules ranges from 200-700 nm (Fig. 2A, frame 4). During anaphase, GFP-IMP1 becomes concentrated on the polar microtubules in the midzone of the mitotic spindle (Fig. 2B).

To examine the dynamics of GFP-IMP1 localization, cells were followed by time-lapse microscopy (Fig. 3A). Localization in interphase cells changed rapidly within 15-20 minutes during extension of lamellipodia. Monitoring of GFP-IMP1 movements showed that granules exhibited a characteristic saltatory and irregular behaviour. The speed of the individual particles ranged from 0.04 to 0.22 μm/s, with an average speed of 0.12 μm/s (Fig. 3B). Some granules coalesced, creating larger granules that subsequently split up into smaller particles. We also determined the speed and direction of movement by bleaching 16 μm of a cytoplasmic extension and subsequently followed granules moving into the bleached area. Transport was bidirectional and, in agreement with the single-particle measurements, the first particles arrived at the center of the bleached area after 80 seconds, corresponding to a maximal speed of ~0.2 μm/s (data not

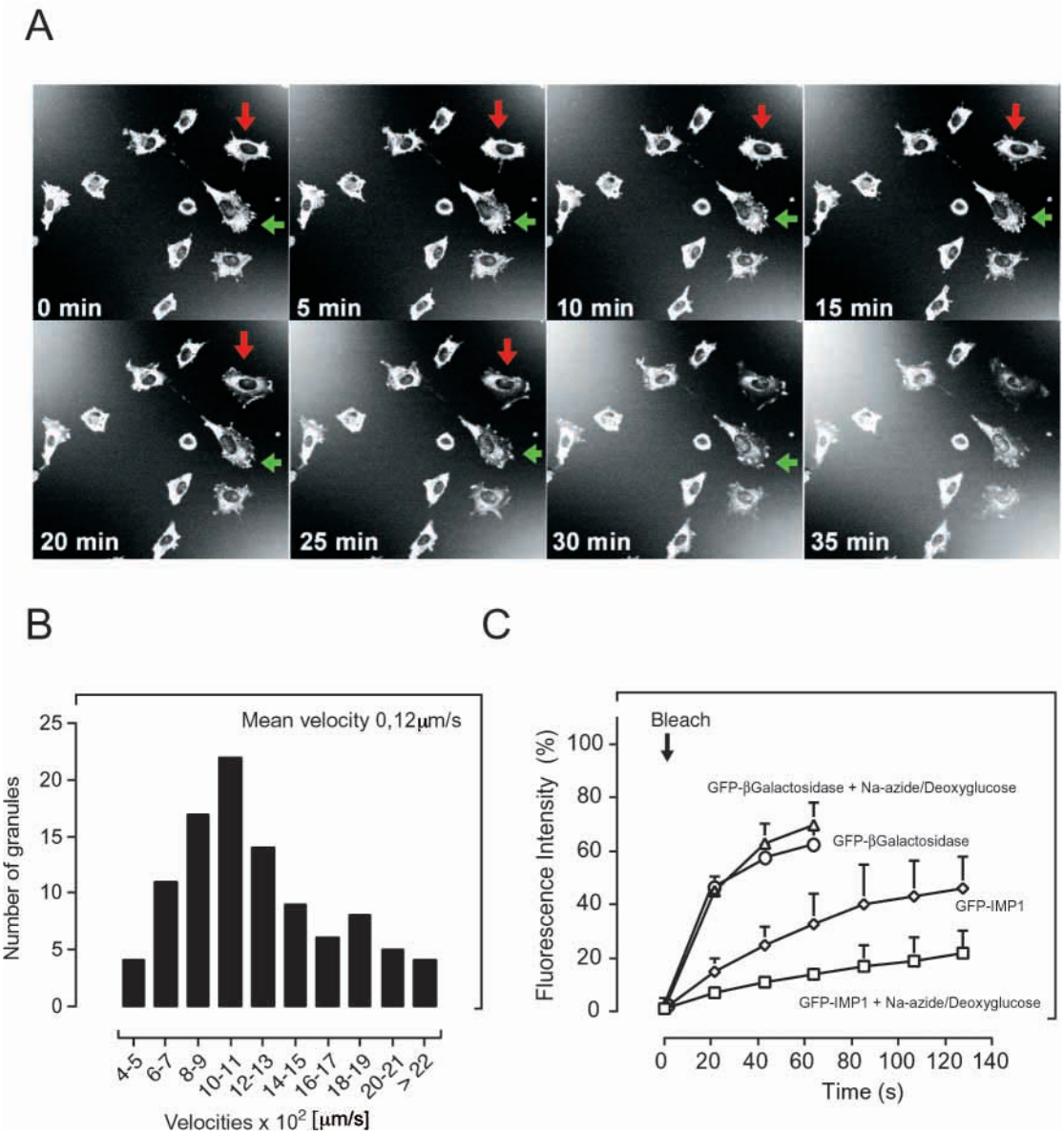

Fig. 3. GFP-IMP1 localization. (A) Time-lapse microscopy of NIH 3T3 cells that stably express GFP-IMP1. Cells with GFP-IMP1 undergoing localization are marked by arrows. (B) Velocity of moving GFP-IMP1 granules. Particles were followed by time-lapse microscopy at 20 second intervals. The velocities of 100 individual particles were calculated by measuring the distance between the particles in two succesive frames. (C) Fluorescence recovery after photobleaching. A cellular extension was bleached, and the transport of GFP-IMP1 into the bleached area was followed by time-lapse microscopy at 20 second intervals in the absence and presence of sodium azide and 2-deoxyglucose. A similar experiment with GFP-β-galactosidase is included as a control.

shown). Half-maximal FRAP was reached after 45 seconds, and the total recovery was ~50% (Fig. 3C). By comparison, the half-maximal recovery of a GFP-β-galactosidase fusion protein took place after 15 seconds, and total recovery was 80%. The presence of sodium azide and 2-deoxyglucose reduced the rate of recovery by a factor of three, suggesting that transport of GFP-IMP1 particles is ATP dependent.

IMP1 is associated with microtubules

As described above, GFP-IMP1 granules are often found in rows, suggesting an association with the cytoskeleton. Moreover, the accumulation of GFP-IMP1 in the midzone during anaphase suggests an association with microtubules. Co-staining of microtubules and GFP-IMP1 in interphase cells showed that GFP-IMP1 granules were distributed along the

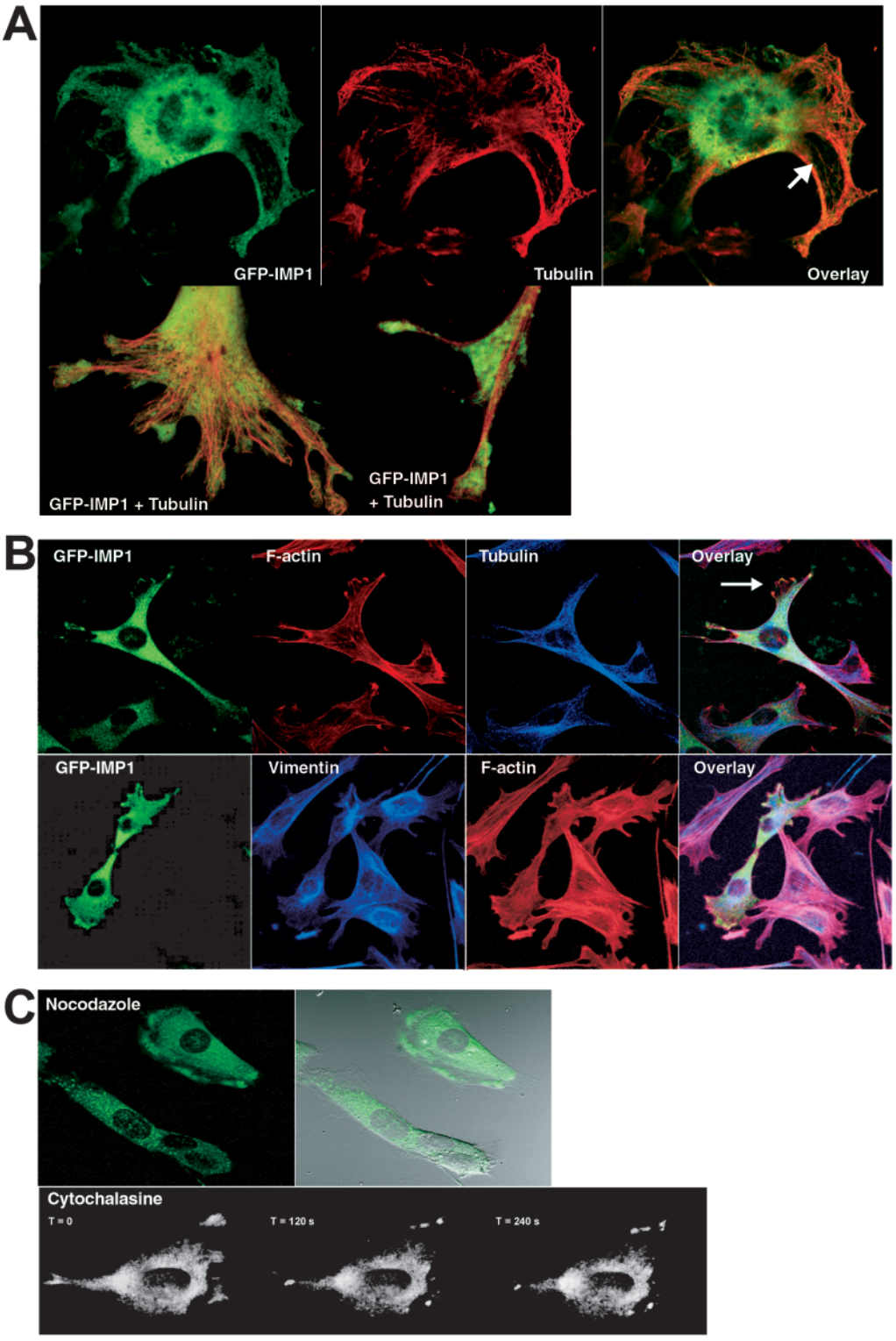

Fig. 4. GFP-IMP1 colocalises with microtubules and F-actin. NIH 3T3 cells that stably express GFP-IMP1 were fixed and stained with anti-tubulin antibody or anti-vimentin and phalloidin and examined by confocal microscopy. (A) The simultaneous detection of GFP-IMP1 (green) and microtubules (red) and their colocalization (arrow). (B, upper panel) The simultaneous detection of GFP-IMP1 (green), microfilaments (red) and microtubules (blue). The arrow in the overlay frame indicates the colocalization of F-actin and GFP-IMP in the lamellipodia. (B, lower panel) The detection of GFP-IMP1 (green), vimentin (blue) and microfilaments (red). (C, upper panel) Cells treated with nocodazole. Most GFP-IMP1 collapses into large aggregates, but a fraction of GFP-IMP1 remains anchored in the lamellipodia for more than 1 hour. (C, lower panel) Time-lapse microscopy of GFP-IMP1 after cytochalasin D treatment. At these short time points, the integrity of the cell is intact, but anchoring in lamellipodia has disappeared.

microtubular network (Fig. 4A,B). Moreover, in the lamellipodia there was a partial overlap between the staining pattern of phalloidin (F-actin) and GFP-IMP-1. We did not observe any particular association with the intermediate filaments. Incubation with nocodazole (10 μg/ml) was followed by collapse and aggregation of GFP-IMP1 in the cytoplasm, but it left a subpopulation of GFP-IMP1 in the lamellipodia unaffected (Fig. 4C). The GFP-IMP1 in the lamellipodia remains attached for more than an hour after nocodazole treatment, suggesting stable microtubule-independent anchoring. Incubation with cytochalasin D (2 μg/ml) caused a rapid (~2 minutes) disappearance of GFP-IMP1 from the lamellipodia (Fig. 4C), indicating that anchoring is connected to microfilaments. After longer incubations (15-20 minutes) a marked disruption of the cellular architecture was noted.

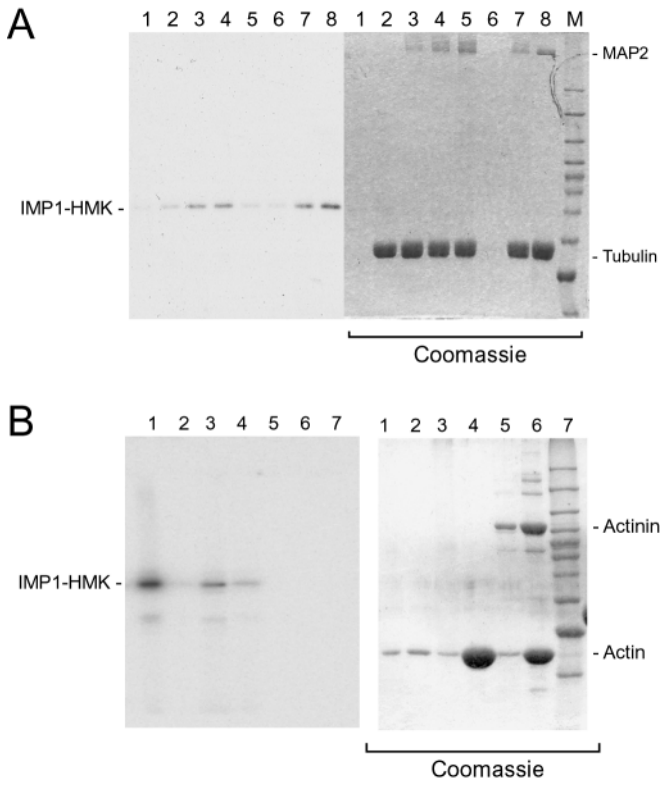

Fig. 5. IMP1 binds to microtubules. (A) ^{32}P-labelled recombinant IMP1-HMK was precipitated with tubulin and microtubule-associated proteins (MAPs) in the presence of paclitaxel and GTP. IMP1-HMK in the presence of buffer (lane 1); polymerised tubulin (lane 2); polymerised tubulin and 1.25 μg total MAPs (lane 3); polymerised tubulin and 2.5 μg total MAPs (lane 4); polymerised tubulin and 5 μg total MAPs and 15 nM leader 3 segment C RNA (lane 5); unpolymerised tubulin and 2.5 μg total MAPs (lane 6); polymerised tubulin and 2.5 μg total MAPs and 2 units RNase T1 (lane 7); polymerised tubulin and 3 μg MAP2 (lane 8). The autoradiograph is on the left, and the Coomassie brilliant blue staining is on the right. M is a molecular mass marker. (B) Pull-down of ^{32}P-labelled IMP1-HMK in the absence of polymerised actin (lane 1, supernatant; lane 2, pellet) or in the presence of polymerised actin (lane 3, supernatant; lane 4, pellet). Pull-down of actinin by polymerised actin (lane 5, supernatant; lane 6, pellet). The autoradiograph is on the left, and the Coomassie brilliant blue-staining is on the right.

To confirm that IMP1 could associate with microtubules, ^{32}P-labelled recombinant IMP1 was incubated with MAP-enriched and paclitaxel-stabilised polymerised tubulin from calf brain and precipitated by centrifugation (Fig. 5A). Whereas IMP1 was efficiently precipitated by MAP-enriched

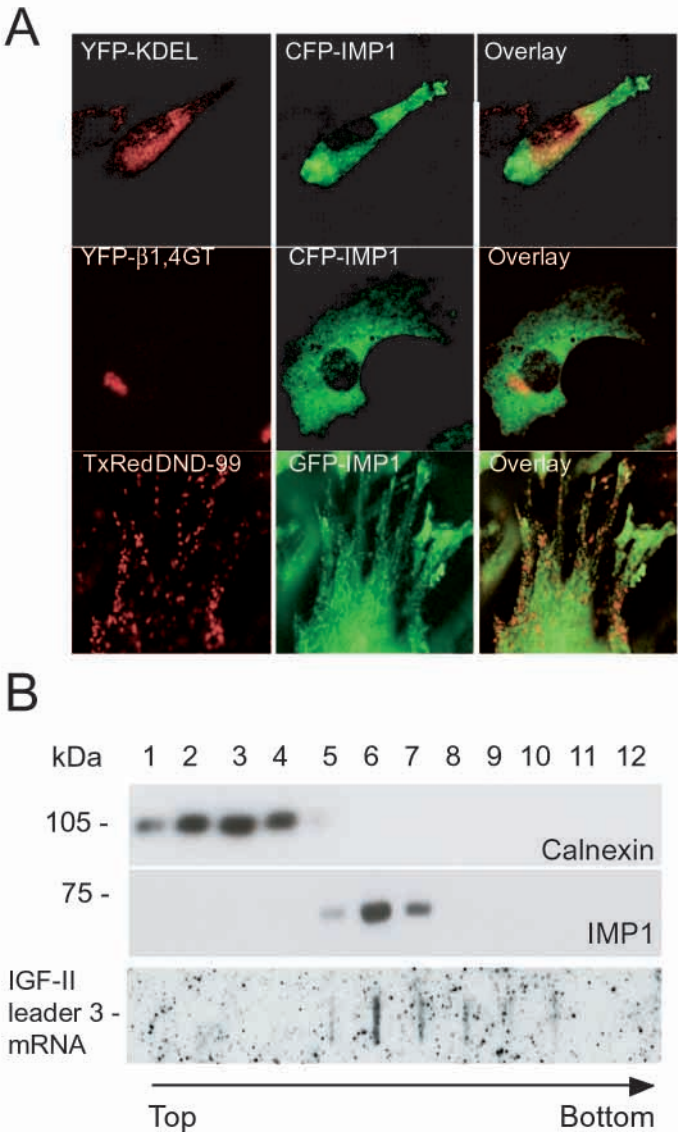

Fig. 6. CFP-IMP1 does not colocalise with membranous compartments. (A) CFP-IMP1 was cotransfected into NIH 3T3 cells together with YFP-linked markers of the endoplasmic reticulum (YFP-KDEL) and Golgi apparatus (YFP-β1,4GT), or GFP-IMP1 was cotransfected with a Texas Red-linked marker for acid vesicles. There is no apparent colocalization of fluorescently tagged IMP1 with any of the markers and, in the cases of the Golgi apparatus and acid vesicles, exclusion is often observed. The pictures from cotransfections with ER and Golgi markers are in pseudo-colours to aid visualisation: YFP fluorescence is shown in red, CFP fluorescence is shown in green, and regions of overlap are shown in yellow. (B, upper and middle panels) Western blot with anti-calnexin and anti-IMP1 antibodies of 12 fractions from a 10-60% Nycodenz sedimentation analysis of an undiluted RD cellular lysate. Positions of molecular mass markers are shown at the left. (B, lower panel) Slot-blot analysis of total RNA from the same fractions with a probe specific for IGF-II leader 3 mRNA.

polymerised tubulin, neither polymerised tubulin in the absence of MAPs nor unpolymerised tubulin in the presence of MAPs was able to precipitate IMP1. To test whether the binding to microtubules was mediated by protein-protein interaction or whether IMP1 was indirectly bound through RNA, precipitation was also carried out in the presence of RNAse T1, which had no effect on IMP1 precipitation. Inclusion of an excess of a high-affinity RNA target from IGF-II mRNA actually prevented precipitation. Moreover, substitution of the MAP fraction with 90% pure MAP2 gave virtually identical results. Finally, we examined the binding of recombinant IMP1 to microfilaments (Fig. 5B). In contrast to actinin, which was efficiently precipitated by actin-filaments, IMP1 was almost exclusively detected in the supernatant. We infer that IMP1 does not associate directly with microfilaments.

In order to examine a possible colocalization of IMP1 with membranous compartments in the mouse fibroblasts, CFP-IMP1 and YFP-linked markers of membranous compartments were cotransfected (Fig. 6A). Colocalization with the markers was neither observed in the cell body nor in the lamellipodia. The lack of membrane association was corroborated by centrifugation analysis of an undiluted RD cellular lysate in a 10-60% Nycodenz gradient (Fig. 6B), where endogenous IMP1-containing RNPs exhibited an apparent density of 1.23 g/ml. The calnexin marker for ER sedimented at an apparent density range of 1.09-1.16 g/ml. Moreover, slot-blot analysis of the Nycodenz gradient fractions with an IGF-II leader 3-specific probe revealed that the translationally repressed 6.0 kb transcript (Nielsen et al., 1995) co-sedimented with endogenous IMP1 (Fig. 6B).

Granule formation and cytoplasmic localization of GFP-IMP1 deletion constructs

IMP1 consists of six putative RNA-binding domains, so to identify the structural determinants necessary for proper granule formation and localization, a series of GFP-IMP1 deletion constructs were transiently expressed in NIH 3T3 cells, and the cytoplasmic appearance was examined by confocal microscopy (Fig. 7A,B). Whereas full-length GFP-IMP1 formed large granules and localized to the lamellipodia, as described above, the two RRM domains were diffuse and were distributed all over the cytoplasm. In contrast, KH domains 1-4 assembled in granules that were distributed in a manner similar to full-length IMP1. Deletion of KH domain 1 or 4 was followed by loss of both granular appearance and anchoring in lamellipodia. In order to examine whether the KH1-4 deletion mutant assembles in the same granules as full-length IMP1, we co-expressed CFP-IMP1 with YFP-KH1-4. Overlay of the two pictures revealed that CFP-IMP1 and YFP-KH1-4 were embedded in the same granules (Fig. 7C). We conclude that the entity comprising the four KH

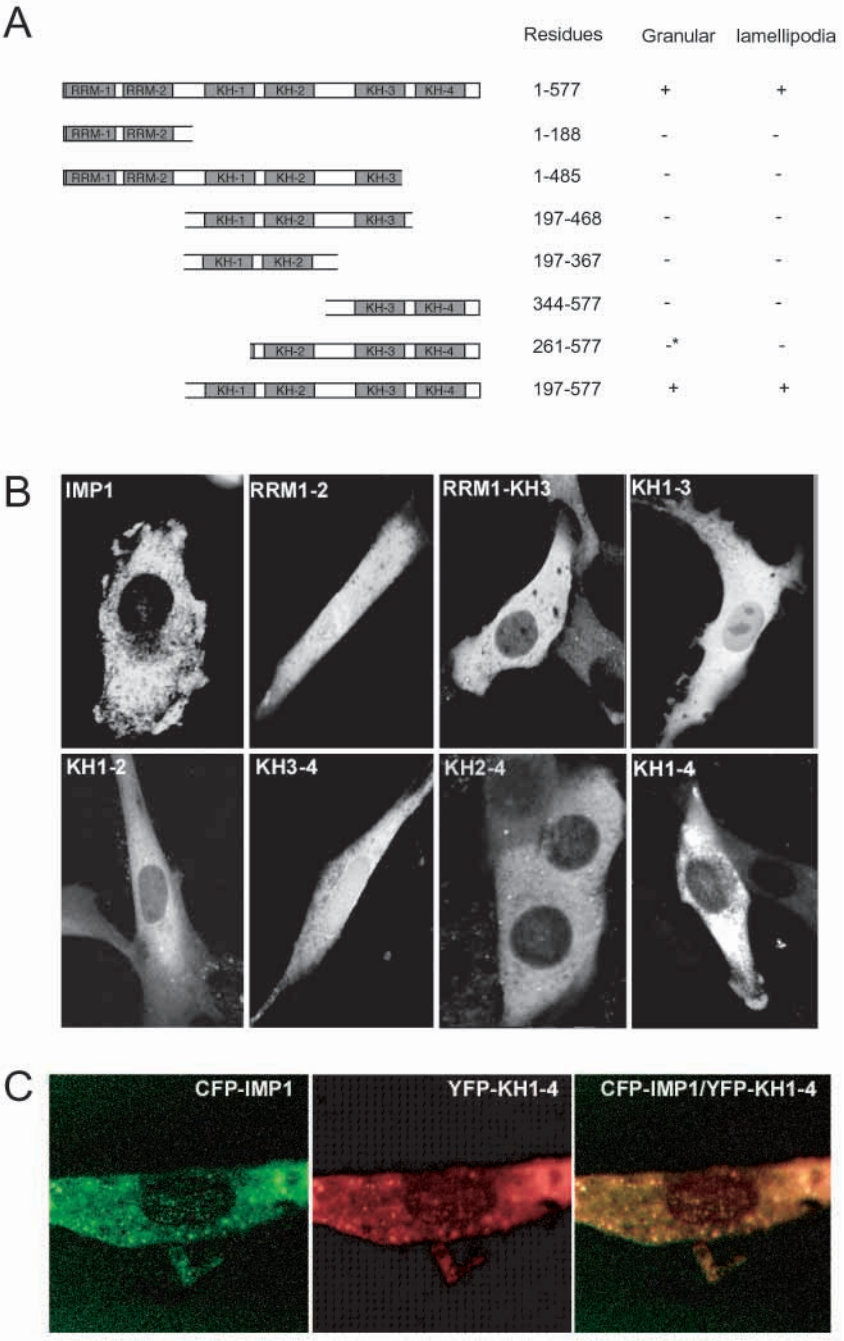

Fig. 7. Subcytoplasmic localization of IMP1 is mediated by the four KH domains. NIH 3T3 cells were transiently transfected with GFP-IMP1 deletion constructs. (A) Schematic representation of the constructs and their ability (+) to form granules and localise subcytoplasmically. *The KH2-4 construct exhibited a tendency to form immobile aggregates that could be mistaken for granules. (B) Representative pictures of the constructs. (C) Cotransfection of CFP-IMP1 and YFP-KH1-4. The frames are in pseudo-colours to aid visualisation: CFP fluorescence is shown in green, YFP fluorescence is shown in red, and regions of overlap are shown in yellow.

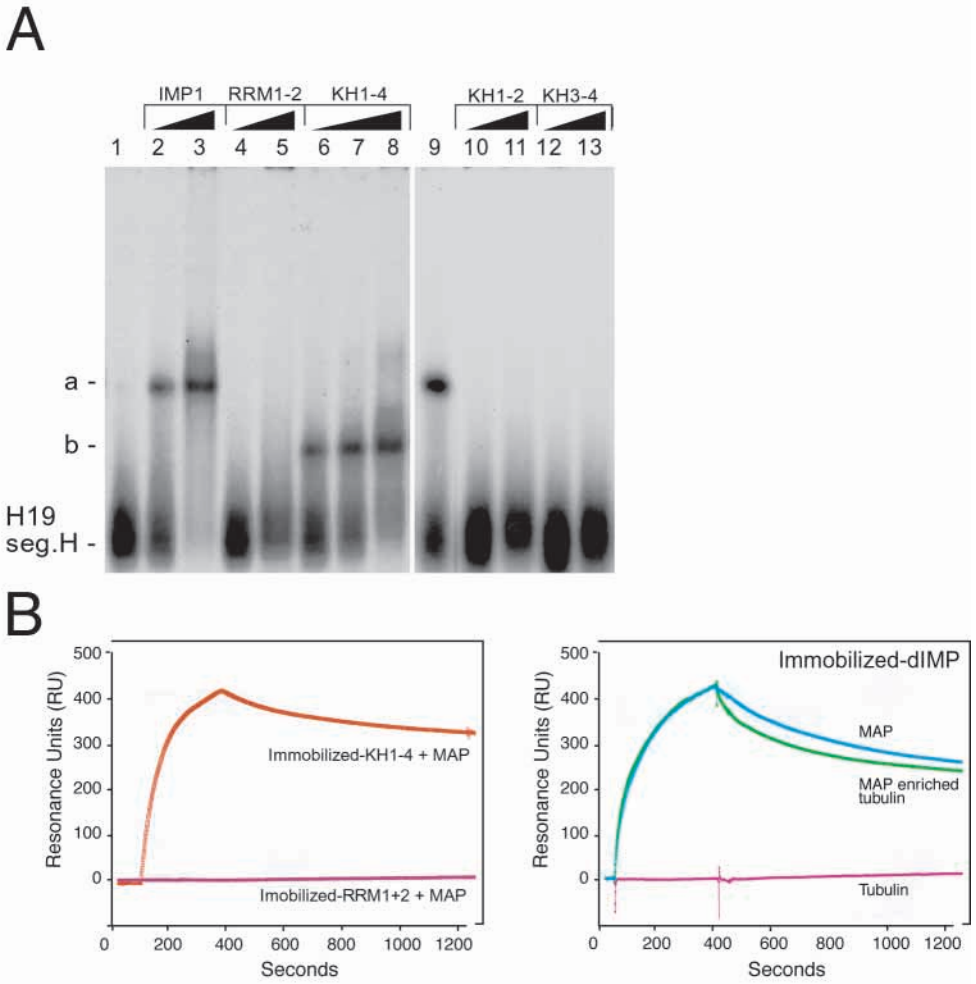

Fig. 8. RNA binding and MAP association are mediated by the KH modules. Autoradiograph from an electrophoretic mobility-shift analysis of ^{32}P-labelled H19 segment H (H19 seg. H) with recombinant IMP-1 (lane 2: 0.3 nM; lane 3: 3 nM; lane 9: 0.6 nM), RRM1-2 (lane 4: 10 nM; lane 5: 100 nM), KH1-4 (lane 6: 0.6 nM; lane 7: 1.2 nM; lane 8: 3 nM), KH1-2 (lane 10: 20 nM; lane 11: 100 nM) and KH3-4 (lane 12: 20 nM; lane 13: 100 nM). The positions of unbound RNA and RNA-protein complexes a and b are shown at the left. (B) Real-time surface plasmon resonance binding of phosphocellulose-purified MAPs to recombinant RRM1-2 and KH1-4 immobilized on a CM5 sensorchip surface (left panel), and binding of phosphocellulose-purified MAPs and MAP-enriched tubulin to immobilized *Drosophila* IMP (right panel).

domains is sufficient for the cytoplasmic trafficking of full-length IMP1.

KH-dependent RNA-binding and microtubule association

We examined the RNA-binding of IMP1 deletions by electrophoretic mobility-shift analysis. Fig. 8A shows an autoradiograph from electrophoresis of the ^{32}P-labelled 173-nucleotide segment H of H19 RNA, which is a high-affinity IMP1 RNA target (Runge et al., 2000), in the presence of increasing concentrations of IMP1, RRM1-2 and KH1-4. Whereas IMP1 and KH1-4 bound to segment H RNA with apparent K_ds of 0.4 nM and 2 nM, respectively, neither the two RRM modules nor the KH1-2 or KH3-4 modules were able to bind to the RNA-target at concentrations of 0.1 μM. We infer that the entity consisting of the four KH domains is the major H19 RNA-binding determinant.

To examine whether the RRMs or the KH domains interacted with the MAP fraction, we tested the binding of RRM1-2 and KH1-4 to phosphocellulose-purified MAPs by surface plasmon resonance. Equimolar amounts of the domains were immobilized on the sensorchip, and a clear interaction was observed between the four KH domains and the MAP fraction (Fig. 8B, left panel). No binding was detectable with the two RRM modules. Finally, we examined the binding of MAPs to *Drosophila* IMP (dIMP), which consists of only the four KH motifs. Whereas immobilized dIMP did not bind to purified tubulin, a distinct binding was obtained with both the MAP-enriched tubulin and the purified MAP preparation (Fig. 8B, right panel), implying that the interaction between the four KH domains and the MAP fraction is phylogenetically conserved.

Discussion

The family of IMP proteins, and their orthologues in chicken and *Xenopus*, has been implicated in the localization of H19, β-actin and Vg1 mRNAs to the leading edges of fibroblast cells and to the vegetal pole of the oocyte during stages III and IV, respectively. Whereas the dynamics of β-actin and Vg1 mRNA localization have been studied in great detail, little is known about the trafficking of the zipcode-binding proteins. In the present study, we have characterised the dynamic cytoplasmic localization of GFP-IMP1 fusion proteins and the structural determinants for proper transport and granule formation.

GFP-IMP1 was cytoplasmic at steady state and present in large granules that were distributed along the microtubular network and in the cortical region of the lamellipodia, similar to β-actin mRNA and H19 RNA (Hill et al., 1994; Latham et al., 1994; Runge et al., 2000). The optical diameter range of 200-700 nm of the granules was similar to that of Staufen- and

myelin basic protein mRNA-containing granules. Trafficking in the interphase cells was highly dynamic and changed within 15-20 minutes during extension of lamellipodia and motility. The fraction of cells that exhibit localization of GFP-IMP1 thus seems to reflect the fraction of the cells that are actively migrating or spreading at a given time point, rather than merely being a random subpopulation of the cells. During anaphase, GFP-IMP1 accumulated at the polar microtubules in the midzone of the mitotic spindle, whereas little, if any, GFP-IMP1 colocalized with the kinetochore or astral microtubules.

IMP1 was able to associate with microtubules, which was in agreement with previous data from Elisha et al. (Elisha et al., 1995), who showed that *Xenopus* Vg1-RBP associated with microtubules, and this may rationalize the predominant localization of GFP-IMP1 to the tightly packed polar microtubules during anaphase. The size of the mobile fraction in the FRAP experiment implies that about half of the GFP-IMP1 is immobilized on microtubules, whereas the other half is in transit by a mechanism that is likely to involve motor proteins. Granules moved in a characteristic saltatory manner in both the plus- and minus-end direction along the microtubular network. The average velocity of 0.12 μm/s is similar to that observed for Staufen-containing granules (Kohrmann et al., 1999) and a number of other RNA-containing granules, such as myelin basic protein mRNA-containing granules (Ainger et al., 1993), suggesting that these RNPs move by a similar, but currently unknown, molecular mechanism. In contrast to Vg1 mRNA and Vg1-RBP/Vera, which have previously been reported to be localized via their microtubule-independent binding to a subcompartment of the endoplasmic reticulum in *Xenopus* oocytes (Deshler et al., 1997; Etkin, 1997; Kloc and Etkin, 1998; Lee and Chen, 1988), GFP-IMP1 does not appear to associate with the ER or other organelles in fibroblasts. Moreover, endogenous IMP1 and IGF-II leader 3 mRNA from RD cells band at the buoyant density of RNP particles in the Nycodenz gradient.

A subpopulation of GFP-IMP1 was anchored at nocodazole-insensitive sites in the lamellipodia. Transport and anchoring are not necessarily linked phenomena, as demonstrated by myelin basic protein mRNA, where one cis-element appears to be necessary for transport and another mediates anchoring (Ainger et al., 1997). Our data are consistent with a model where IMP travels with its RNA cargo and becomes anchored via a putative adaptor protein to filaments in the cortical region of the lamellipodia, implying that the same cis-element mediates both events. β-actin mRNA localization in chicken embryo fibroblasts has previously been reported to be disrupted by cytochalasin D, indicating that β-actin mRNA localization in these cells is connected to microfilaments (Sundell and Singer, 1991). In the *Xenopus* oocyte, Vg1 mRNA is also anchored at the vegetal pole in a microfilament-dependent manner (Yisraeli et al., 1990).

Deletion analysis of IMP1 revealed that the four KH domains, but not the two RRMs, are sufficient for both intracellular granule formation and trafficking of IMP1, as well as RNA binding in vitro. The maxi-KH domain is an autonomously folded unit of about 70 amino acids with βααββα topology, which is present in a wide variety of proteins, often in multiple copies, with the 15 repeats in vigilin and its yeast homologue (Scp160) as an extreme. A common property among members of the KH family is their RNA-binding ability, but the present study strongly suggests that they are multifunctional motifs. Although it could be argued that the regions between the four KH domains in the KH1-4 deletion mutant could mediate the biological effects in terms of RNA trafficking, their small sizes and non-conserved sequences make this unlikely. When the third KH domain from the human Nova antigen was crystallized, it formed an intermolecular tetramer (Lewis et al., 1999), suggesting that the KH domain may have an inherent ability to oligomerize. The function of the two RRMs in the vertebrate branch of the family is currently unclear. Although the two RRMs on their own cannot bind to the high-affinity H19 RNA-target, they nevertheless contribute to a lower K_d in the full-length molecule.

The three aspects of IMP1 localization – RNA-binding, granule formation and anchoring in lamellipodia – could not be separated in the present deletion analysis, suggesting that they are interdependent. A plausible explanation is that RNA-binding and granule formation are prerequisites for subsequent transport, possibly through a cumulative effect. This interpretation is supported by the narrow density distribution of IMP-RNP in the Nycodenz gradient, which implies that in spite of a broad range of particle sizes, the RNA-protein ratio in the particles is constant. Each granule must contain many GFP-IMP1 molecules (otherwise they would not appear as visible granules), and this high local concentration of IMP1 in a 'burr'-like structure could lead to a much higher association rate of the granule to the localization apparatus than single IMP1 molecules would exhibit. The motifs needed for localization and granule formation of IMP1 – as well as for efficient attachment of RNA cargo – are situated within the conserved part of the protein, since both the recently characterised *Drosophila* IMP homologue and the apparent IMP homologue from *C. elegans* (accession number T23837) consist of four KH domains and no RRMs.

We thank Lena B. Johansson, Bente Rotbøl and Joan Christiansen for technical assistance. The research was supported by the Danish Natural Science and Medical Research Councils, the Danish Cancer Society, the Novo Nordisk Foundation and the Toyota Foundation.

References

Ainger, K., Avossa, D., Diana, A. S., Barry, C., Barbarese, E. and Carson, J. H. (1997). Transport and localization elements in myelin basic protein mRNA. *J. Cell Biol.* **138**, 1077-1087.

Ainger, K., Avossa, D., Morgan, F., Hill, S. J., Barry, C., Barbarese, E. and Carson, J. H. (1993). Transport and localization of exogenous myelin basic protein mRNA microinjected into oligodendrocytes. *J. Cell Biol.* **123**, 431-441.

Deshler, J. O., Highett, M. I., Abramson, T. and Schnapp, B. J. (1998). A highly conserved RNA-binding protein for cytoplasmic mRNA localization in vertebrates. *Curr. Biol.* **8**, 489-496.

Deshler, J. O., Highett, M. I. and Schnapp, B. J. (1997). Localization of *Xenopus* Vg1 mRNA by Vera protein and the endoplasmic reticulum. *Science* **276**, 1128-1131.

Doyle, G. A., Betz, N. A., Leeds, P. F., Fleisig, A. J., Prokipcak, R. D. and Ross, J. (1998). The c-myc coding region determinant-binding protein: a member of a family of KH domain RNA-binding proteins. *Nucleic Acids Res.* **26**, 5036-5044.

Elisha, Z., Havin, L., Ringel, I. and Yisraeli, J. K. (1995). Vg1 RNA binding protein mediates the association of Vg1 RNA with microtubules in Xenopus oocytes. *EMBO J.* **14**, 5109-5114.

Etkin, L. D. (1997). A new face for the endoplasmic reticulum: RNA localization. *Science* **276**, 1092-1093.

Havin, L., Git, A., Elisha, Z., Oberman, F., Yaniv, K., Schwartz, S. P., Standart, N. and Yisraeli, J. K. (1998). RNA-binding protein conserved

in both microtubule- and microfilament-based RNA localization. *Genes Dev.* **12**, 1593-1598.

Hill, M. A., Schedlich, L. and Gunning, P. (1994). Serum-induced signal transduction determines the peripheral location of beta-actin mRNA within the cell. *J. Cell Biol.* **126**, 1221-1229.

Hoek, K. S., Kidd, G. J., Carson, J. H. and Smith, R. (1998). hnRNP A2 selectively binds the cytoplasmic transport sequence of myelin basic protein mRNA. *Biochemistry* **37**, 7021-7029.

Jensen, T. H., Leffers, H. and Kjems, J. (1995). Intermolecular binding sites of human immunodeficiency virus type 1 Rev protein determined by protein footprinting. *J. Biol. Chem.* **270**, 13777-13784.

Kloc, M. and Etkin, L. D. (1998). Apparent continuity between the messenger transport organizer and late RNA localization pathways during oogenesis in *Xenopus*. *Mech. Dev.* **73**, 95-106.

Kohrmann, M., Luo, M., Kaether, C., DesGroseillers, L., Dotti, C. G. and Kiebler, M. A. (1999). Microtubule-dependent recruitment of Staufen-green fluorescent protein into large RNA-containing granules and subsequent dendritic transport in living hippocampal neurons. *Mol. Biol. Cell* **10**, 2945-2953.

Kwon, S. and Schnapp, B. J. (2001). RNA localization: SHEdding light on the RNA-motor linkage. *Curr. Biol.* **11**, R166-R168.

Latham, V. M., Jr., Kislauskis, E. H., Singer, R. H. and Ross, A. F. (1994). Beta-actin mRNA localization is regulated by signal transduction mechanisms. *J. Cell Biol.* **126**, 1211-1219.

Lee, C. and Chen, L. B. (1988). Dynamic behavior of endoplasmic reticulum in living cells. *Cell* **54**, 37-46.

Lewis, H. A., Chen, H., Edo, C., Buckanovich, R. J., Yang, Y. Y., Musunuru, K., Zhong, R., Darnell, R. B. and Burley, S. K. (1999). Crystal structures of Nova-1 and Nova-2 K-homology RNA-binding domains. *Structure Fold. Des.* **7**, 191-203.

Morgenstern, J. P. and Land, H. (1990). Advanced mammalian gene transfer: high titre retroviral vectors with multiple drug selection markers and a complementary helper-free packaging cell line. *Nucleic Acids Res.* **18**, 3587-3596.

Nielsen, F. C., Østergaard, L., Nielsen, J. and Christiansen, J. (1995). Growth-dependent translation of IGF-II mRNA by a rapamycin-sensitive pathway. *Nature* **377**, 358-362.

Nielsen, J., Christiansen, J., Lykke-Andersen, J., Johnsen, A. H., Wewer, U. M. and Nielsen, F. C. (1999). A family of insulin-like growth factor II mRNA-binding proteins represses translation in late development. *Mol. Cell. Biol.* **19**, 1262-1270.

Nielsen, J., Nielsen, F. C., Kragh Jakobsen, R. and Christiansen, J. (2000). The biphasic expression of IMP/Vg1-RBP is conserved between vertebrates and *Drosophila*. *Mech. Dev.* **96**, 129-132.

Ross, A. F., Oleynikov, Y., Kislauskis, E. H., Taneja, K. L. and Singer, R. H. (1997). Characterization of a beta-actin mRNA zipcode-binding protein. *Mol. Cell. Biol.* **17**, 2158-2165.

Runge, S., Nielsen, F. C., Nielsen, J., Lykke-Andersen, J., Wewer, U. M. and Christiansen, J. (2000). H19 RNA binds four molecules of insulin-like growth factor II mRNA-binding protein. *J. Biol. Chem.* **275**, 29562-29569.

Spring, J. (1997). Vertebrate evolution by interspecific hybridisation–are we polyploid? *FEBS Lett.* **400**, 2-8.

St Johnston, D., Beuchle, D. and Nusslein-Volhard, C. (1991). *Staufen*, a gene required to localize maternal RNAs in the *Drosophila* egg. *Cell* **66**, 51-63.

Sundell, C. L. and Singer, R. H. (1991). Requirement of microfilaments in sorting of actin messenger RNA. *Science* **253**, 1275-1277.

van Eeden, F. and St Johnston, D. (1999). The polarisation of the anterior-posterior and dorsal-ventral axes during *Drosophila* oogenesis. *Curr. Opin. Genet. Dev.* **9**, 396-404.

Yisraeli, J. K., Sokol, S. and Melton, D. A. (1990). A two-step model for the localization of maternal mRNA in *Xenopus* oocytes: involvement of microtubules and microfilaments in the translocation and anchoring of Vg1 mRNA. *Development* **108**, 289-298.